DOE-ER02712-8
old COO-2712-8

STUDIES OF MECHANICAL PROPERTIES AND IRRADIATION DAMAGE NUCLEATION OF HTGR GRAPHITES

FINAL REPORT

May 1981

P. A. THROWER

The Pennsylvania State University
University Park, Pennsylvania 16802

PREPARED FOR

U.S. Department of Energy

Under Contract No. DE-AC02-76ER02712. M004

NOTICE

A. Personnel and Tasks

The following persons worked on the project:--

P. A. Thrower, principal investigator: electron microscopy of irradiated graphites; oxidation and strength studies.

D. R. Marx, graduate student (Ph.D.). Studies of the effect of stress on graphite oxidation in air, CO_2 and H_2O. Oxidation of graphite by CO_2 at atmospheric pressure.

J. C. Bognet, graduate student (M.S.). Studies of the effect of oxidation in air, CO_2 and H_2O on a variety of commercial graphites.

G. K. Mathew, graduate student (M.S.). Studies of the effect of oxidation on the compressive strength of graphites doped with iron and vanadium.

N. J. McGinnis and T. J. Jesberger, undergraduate seniors. Studies of the effect of oxidation on the compressive strength of graphites doped with calcium.

B. Results obtained since last report

Since the submission of the last report (COO-2712-6) work has concentrated on the examination of the effects of oxidation on the compressive strengths of graphites doped with iron, vanadium and calcium. The purpose of the investigation was to determine the relative effects of the impurities on the rates of oxidation in air, CO_2 and H_2O and the resultant reduction in compressive strength.

1. Materials

The graphites used were manufactured at the Oak Ridge National Laboratory. Each material was provided in the form of a cylinder approximately 3" in diameter and 3" long from which the compression test samples were cut.

Materials containing iron were made from a special low sulfur A-240 petroleum pitch (Ashland Oil Co.). The pitch was coked at 495°C and calcined to 1000°C before grinding. The particle size was limited to a maximum of 1000 μm by screening the product from a hammer mill. In order to obtain reasonable densities about 25% of the filler was given a single pass through

a smaller hammer mill. This improved the particle size distribution for better packing. Iron was added in the form of Fe_2O_3 in the binder which was also A-240 but with a 2.7% sulfur content. No additions of Fe_2O_3 were made to the low-iron grade, while 2% Fe_2O_3 was added to the high-iron grade.

After molding, the blocks were baked at 850°C and then impregnated with the 2.7% S A-240 pitch. Two impregnation cycles were performed. The blocks were then graphitized to 2500°C.

The materials doped with vanadium and calcium were manufactured using similar techniques except that the V_2O_5 or CaO was added to a 2% S A-240 pitch before coking so that the impurity levels after coking were about 0.1% and 0.5% of metal impurity and 1.5% sulfur. In these cases the metallic impurity was added in the manufacture of the filler particles rather than to the binder, as in the case of the iron-containing materials.

2. Physical Properties and Characterization of Materials

Table I shows some of the measured physical properties of the graphites used in the investigation. In all except the materials containing iron bulk density was fairly uniform with values between 1.71 to 1.76 gm cm^{-3}. Compressive strength of the calcium-doped graphites was significantly higher (6500 psi) than for those doped with iron and vanadium (5500-5900 psi). Electrical resistance varied considerably throughout the samples, but there appeared to be little significant difference between the six materials.

Chemical analyses of the materials by semi-quantitative spectrochemical techniques are shown in Table II. All impurities listed are known to act as catalysts in graphite oxidation.

In the low-iron grade the iron content varied from 100 to 150 ppm whereas in the high-iron material a much larger variation was observed. At the edges of the block it was as low as 10 ppm, increasing to 1000 ppm at the center. Concentration variations were also observed in the vanadium-

doped materials while those doped with calcium seemed to show a fairly uniform calcium concentration. In any event these variations showed no precise correlation with any observed effects, possibly because samples from the edges of the block were avoided in the investigation.

Porosimetry measurements using a mercury porosimeter were obtained up to pressures of 30,000 psi, corresponding to pore entrance diameters $\geq$0.006 μm. Porosimeter penetration versus pressure curves are shown in Figure 1 with the differential curves in Figure 2. In all cases the pore volume is almost exclusively contained in pores larger than 1 μm with most of this volume in pores larger than 5 μm. This type of pore distribution is similar to that of the Greak Lakes H-440 graphite reported on earlier. The large amount of very open porosity is to be expected considering the coarse grain size of the filler particles used in fabrication, in spite of the double impregnation used.

Scanning electron microscopy of the fracture surfaces of unoxidized materials showed great similarity between them with no obvious distinction between binder and filler. Cracks and pores of a wide range of sizes were clearly visible, thus accounting for the relatively low strength of these materials. The presence of many clean cleavage surfaces indicated substantial crystal alignment in the precursor.

X-ray diffraction showed that the materials were relatively well graphitized with interlayer spacings of 3.367 ± 0.002 Å and crystallite sizes perpendicular to the layers of 1000 ± 100 Å. The uniformity of the results indicates that the added impurities have not affected the state of graphitization of the materials. This should therefore not be a factor in the investigation.

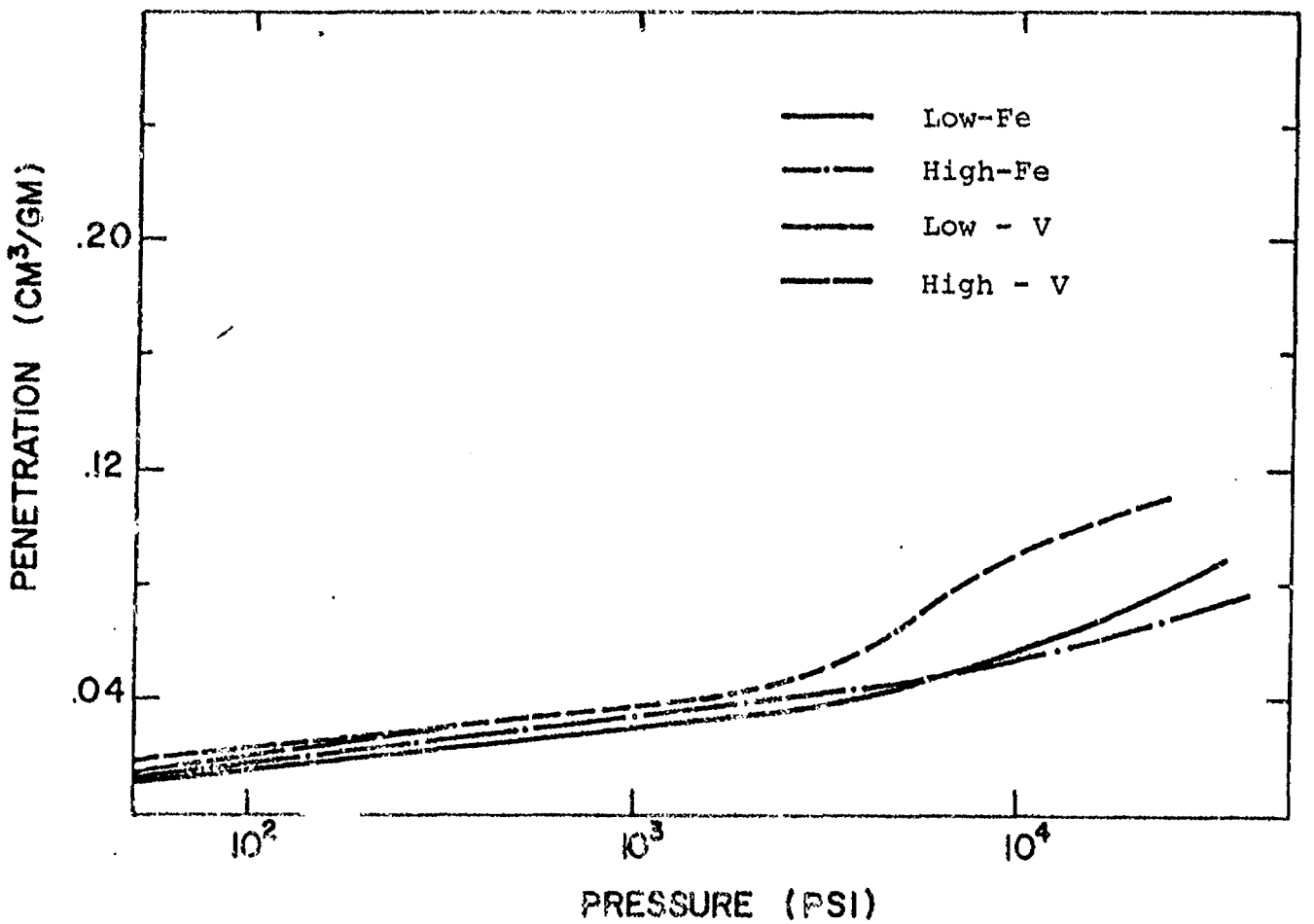

Figure 1. Porosity of unoxidized graphites as a function of mercury porosimeter pressure.

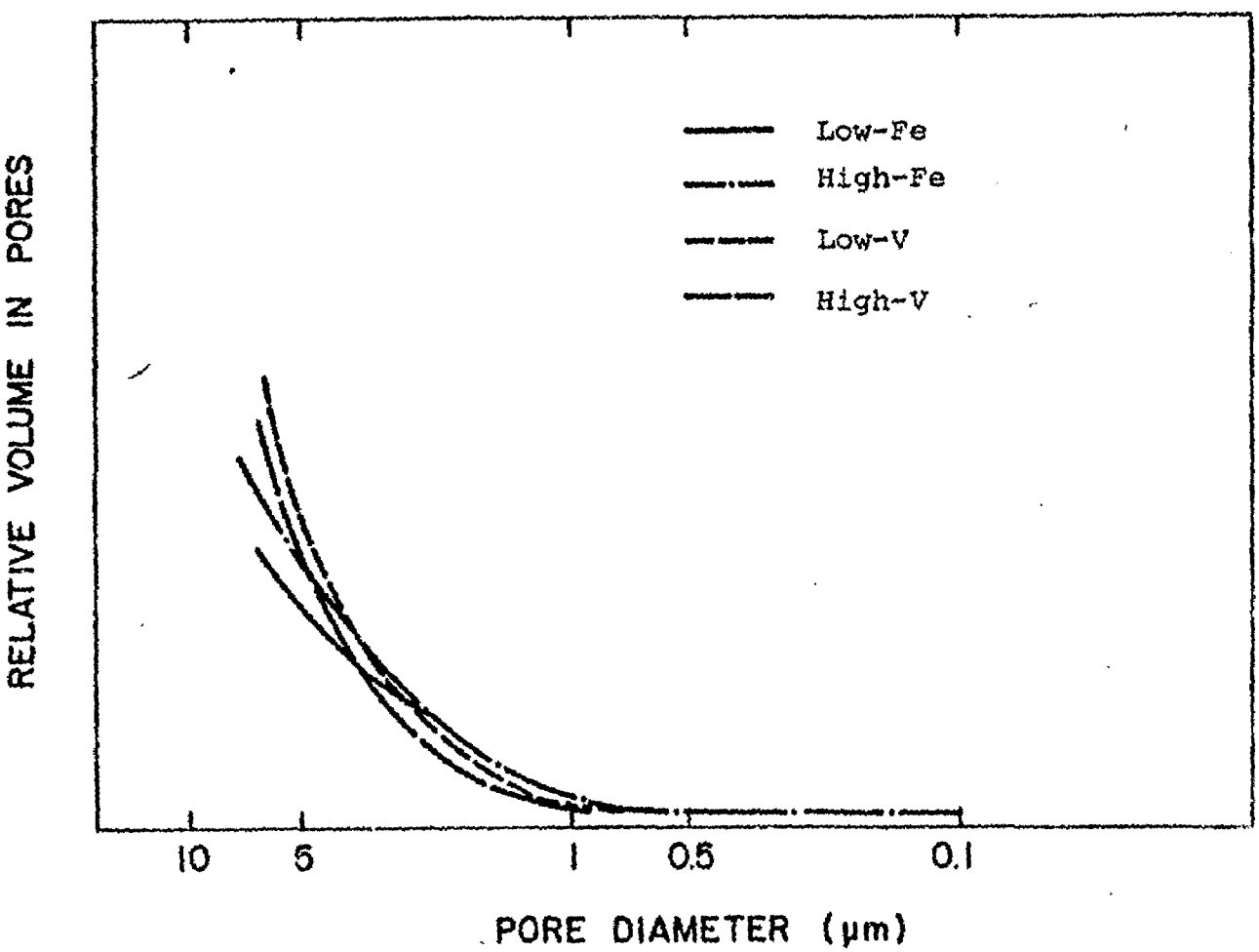

Figure 2. Pore size distributions of unoxidized graphites.

TABLE I

Physical Properties of Graphites

Material ORNL Code	Low Fe (91-23)	High Fe (91-25	Low V (95-37)	High V (95-44)	Low Ca (95-18)	High Ca (95-28)
Density (gm/cm^3)	1.80	1.82	1.71	1.74	1.72	1.74
Compressive Strength (10^3psi)	5.7	5.7	5.5	5.9	6.5	6.7
Electrical Resistivity ($\mu\Omega$-m)	7.4- 9.2	7.6- 9.9	8.6- 11.8	8.4- 10.9	8.4- 12.2	7.9- 11.2
Young's Modulus (10^5psi)	2.55	2.55	2.55	2.60	2.65	2.75

TABLE II

Semi-Quantitative Spectrographic Analysis of Graphites

	Low Fe	High Fe	Low V	High V	Low Ca	High Ca
Fe	100-150	10-1000	30	30	20	5
V	---	---	60-300	300-700	10	5
Ca	20	10	5	30	50	200
Al	40	5	5	---	200	40
Ti	10	5	---	---	20	10
Mg	10	< 2	100	30	10	1
Ba	30	<10	---	---	---	---
Si	100	10	20	20	50	2

Procedure

The blocks of graphite were machined to provide cylindrical compression test samples 0.25" diameter x 0.50" long with a tolerance of ± 0.0015". A typical sample weight was 0.66 gm.

All oxidations were performed at atmospheric pressure. The gases used were dry air, a mixture of equal parts of CO_2 and He, and a mixture of H_2O and He. The last of these was obtained by saturating helium with water by passing it through a fritted disc into a gas washing bottle filled with water. The water temperature was controlled by immersing the bottle in a constant temperature bath. For the iron and vanadium doped materials this was at 40 ± 0.5°C with a resulting water vapor pressure of 55 mm Hg. For the calcium doped graphites the temperature was 30 ± 0.5°C, corresponding to a H_2O vapor pressure of 32 Hg. In all instances the reaction conditions were adjusted to give a reasonable reaction rate while maintaining the original dimensions of the sample, i.e. to keep oxidation uniform throughout the sample. The lower H_2O concentration used for Ca-doped materials was found to be necessary to obtain reaction rates similar to those obtained for the other materials. Typical reaction conditions are given in Table III.

Testing techniques have been described in earlier reports. Compression testing was performed as specified by ASTM standard C695-75 "Compressive (crushing) Strength of Graphite". Fracture stresses were calculated using the original cross sectional area of the sample. In all instances except for CO_2 oxidations, specimens with more than 40% weight loss did show slight reductions in diameter but this range is of little interest as strength loss is almost complete by this time.

RESULTS

1. Reaction Rates

Typical reaction rates for the six graphites are given in Table III. In CO_2, catalytic activity increased in the order V, Ca, Fe, in H_2O V & Fe were

TABLE III

Typical Reaction Conditions and Reaction Rates

Material	Oxidizing Gas	Temperature (°C)	Reaction Rate* (gm/hr)
Low Fe	CO_2	800–900	0.02–0.06
	H_2O	1000	0.05
	Air	500–600	0.01–0.03
High Fe	CO_2	800–900	0.01–0.02
	H_2O	1000	0.04
	Air	550	0.01
Low V	CO_2	850–950	0.01
	H_2O	850–950	0.01
	Air	600–700	0.01–0.06
High V	CO_2	950	0.01
	H_2O	900–1000	0.01–0.03
	Air	600–700	0.03–0.10
Low Ca	CO_2	875	0.015
	H_2O	600	0.01
	Air	500	0.015
High Ca	CO_2	875	0.02
	H_2O	600	0.01
	Air	550	0.015

*Higher rates are for higher temperatures.

about equal with Ca much more active, while in air V seemed to be slightly less active than Fe and Ca.

The most dramatic observation by far was the fact that in order to obtain suitable oxidation of the calcium-doped materials in H_2O it was necessary to reduce the H_2O concentration by 40% and the temperature by 300-400°C from the conditions used for the other materials. The influence of calcium on the oxidation of graphite in H_2O was no less than dramatic and several attempts had to be made in order to produce a reaction which was almost purely chemically controlled, i.e. with no oxidation gradient through the sample.

2. Compression Tests

The reduction of compressive strength was approximately exponential in all cases. Plots of the logarithm of the fracture stress ($\log_{10} \sigma_c$) versus % burn-off (β) are linear within experimental error. Some examples are shown in Figures 3-6. Rather than show all the data points for all 18 experimental investigations it is convenient to express the results in terms of two parameters. The first is obtained by expressing the exponential decrease of compressive strength with burn-off by the formula $\sigma_c/\sigma_o = \exp(-\varepsilon\beta)$ where σ_o is the initial strength and ε is a constant for the reaction conditions. Values of ε have been evaluated and are given in Table IV. The higher the value of ε the greater the reduction of strength produced by a given burn-off.

The second parameter used as a measure of the effect of the oxidation is the percent oxidation (β_{50}) which produces a 50% strength reduction. Values are given in Table V. Theoretically $\beta_{50} = 0.69\varepsilon^{-1}$ and in general the values given in Tables IV & V are in agreement with this relationship.

Strain-to-failure as a function of burn-off for the three oxidation conditions was measured. Values ranged from 4-6% in most cases but often showed a

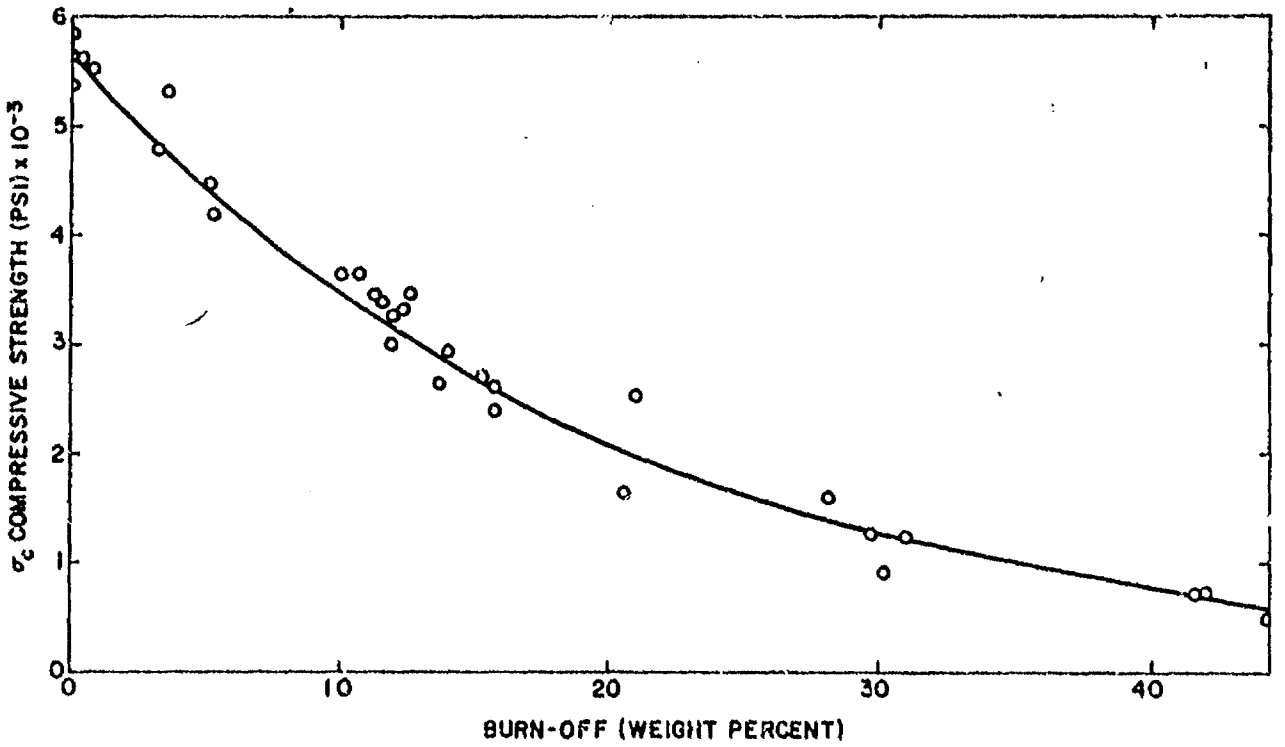

Figure 3. Compressive strength of 91-25 (high-Fe) as a function of burn-off in CO_2.

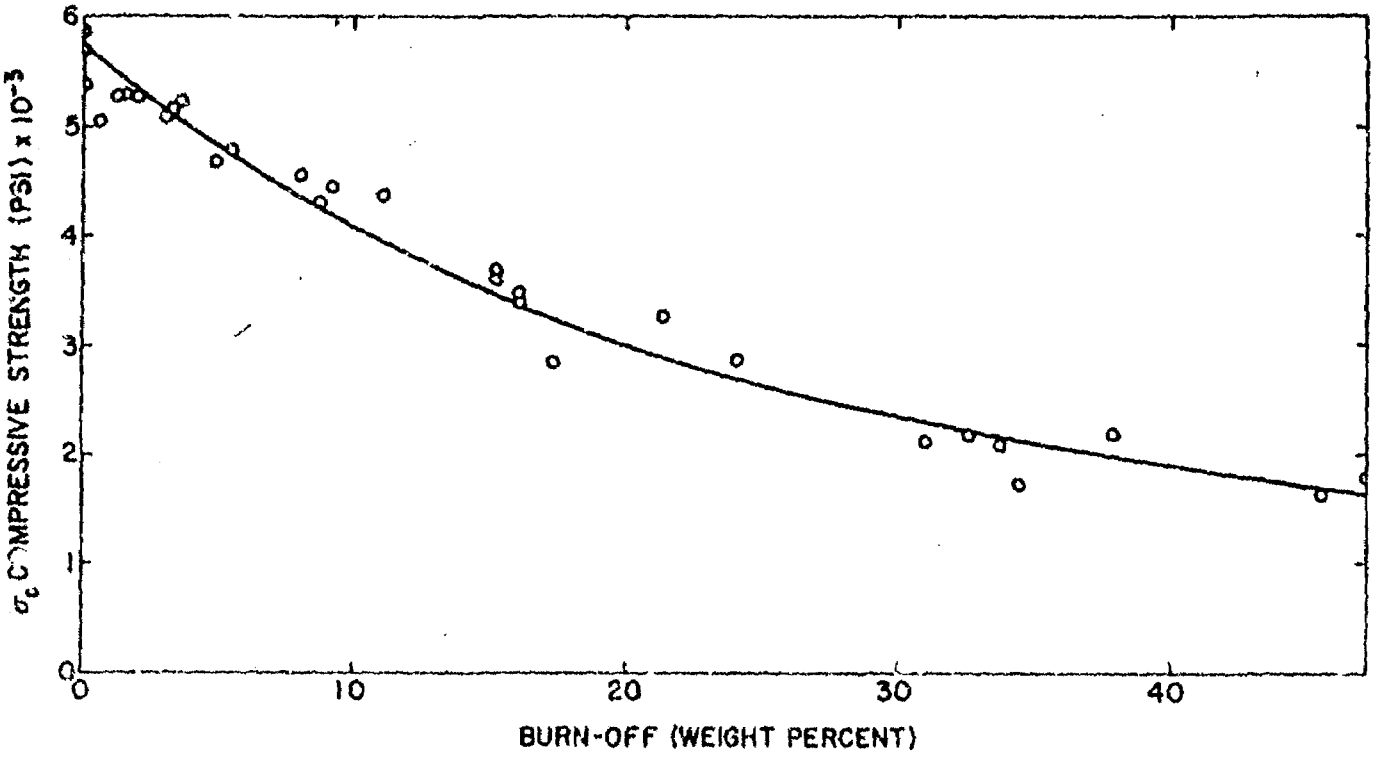

Figure 4. Compressive strength of 91-25 (high-Fe) as a function of burn-off in steam.

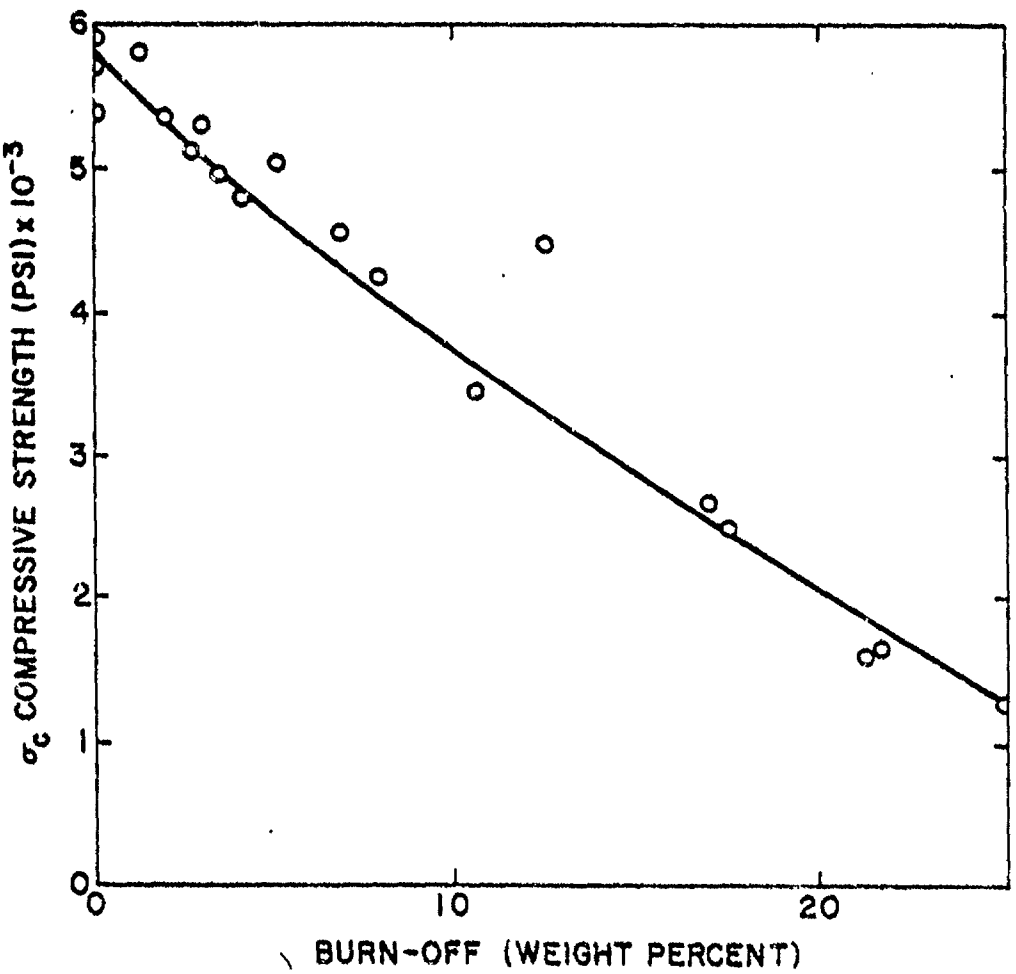

Figure 5. Compressive strength of 91-25 (high-Fe) as a function of burn-off in air.

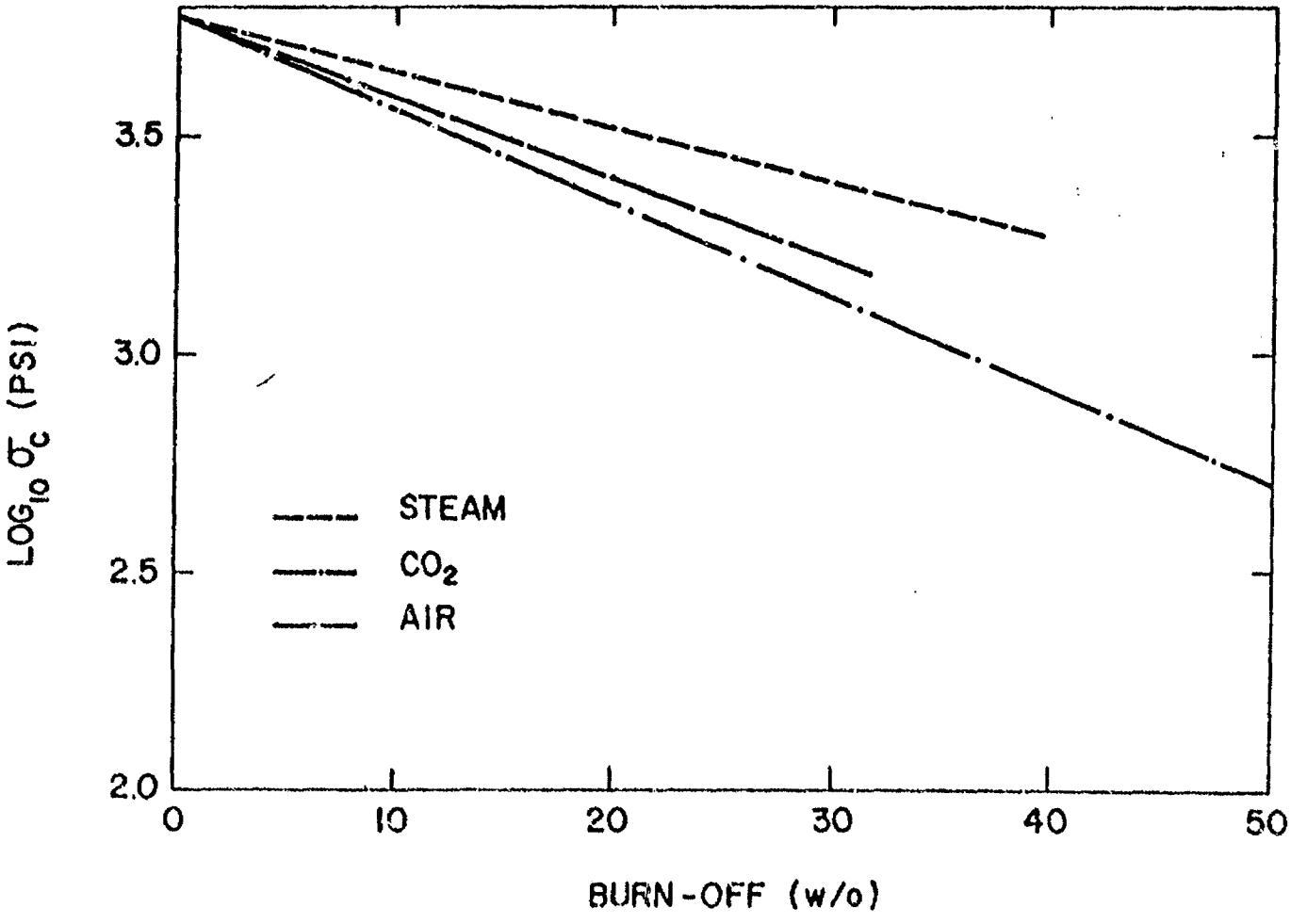

Figure 6. Logarithm of compressive strength of 91-23 (low-Fe) versus burn-off in CO_2, steam and air.

TABLE IV

Values of ε in the expression $\sigma_c/\sigma_o = \exp(-\varepsilon\beta)$

Material	CO_2	Air	H_2O
Low Fe	0.048	0.044	0.025
High Fe	0.053	0.046	0.028
Low V	0.083	0.067	0.035
High V	0.069	0.046	0.069
Low Ca	0.074	0.090	0.088
High Ca	0.060	0.088	0.089

TABLE V

Burn-Off (%) Required to Produce a 50% Loss in Compressive Strength

Material	CO_2	Air	H_2O
Low Fe	15	16	20
High Fe	14	15	20
Low V	10	10	13
High V	11	14	13
High Ca	9	7	7
Low Ca	12	7	7

decrease to 3-4% for the higher burn-offs. Samples cut parallel to the cylinder axis of the original block usually had higher strains-to-failure than those cut perpendicular to the cylinder axis.

Young's moduli were calculated from the initial slopes of the stress-strain curves. Here again there were rapid decreases in the initial stages of oxidation and the changes could be described as an exponential decrease with respect to burn off. Typical linear and logarithmic plots are shown in Figures 7 & 8. Expressing the ratio of the instantaneous Young's modulus (Y) to its value in the unoxidized material (Y_o) as $Y/Y_o = \exp(-\eta\beta)$ where η is a constant, the values of η could be evaluated, and are given in Table VI. Burn-offs which produced a 50% reduction in modulus are shown in Table VII.

A comparison of Tables IV and VI shows that, for oxidations in air and H_2O, η is equal to or greater than ε except for the oxidation of low-Ca material in air. For oxidations in CO_2 this was also true except in three cases (low- and high-Fe and high-Ca) where the logarithmic plots had two linear parts with the region below 25% burn-off giving $\eta < \varepsilon$, while for $\beta > 25\%$ the situation was reversed.

In any event it is certain that the reduction in Young's modulus is at least as rapid as the reduction of compressive strength and in most cases is significantly greater. This fact is further demonstrated by comparing Tables V and VII, where in all cases, except for Fe-doped samples oxidized in CO_2, a 50% reduction in modulus occurs for a lower burn-off than required to produce a 50% reduction in strength.

3. Porosimeter Measurements

Because the pore structures of the original materials were not significantly different it was thought that the differences in oxidation behavior demonstrated in Tables IV-VII might be related to differences in the pore spectra of the oxidized materials. Samples of each graphite with burn-offs

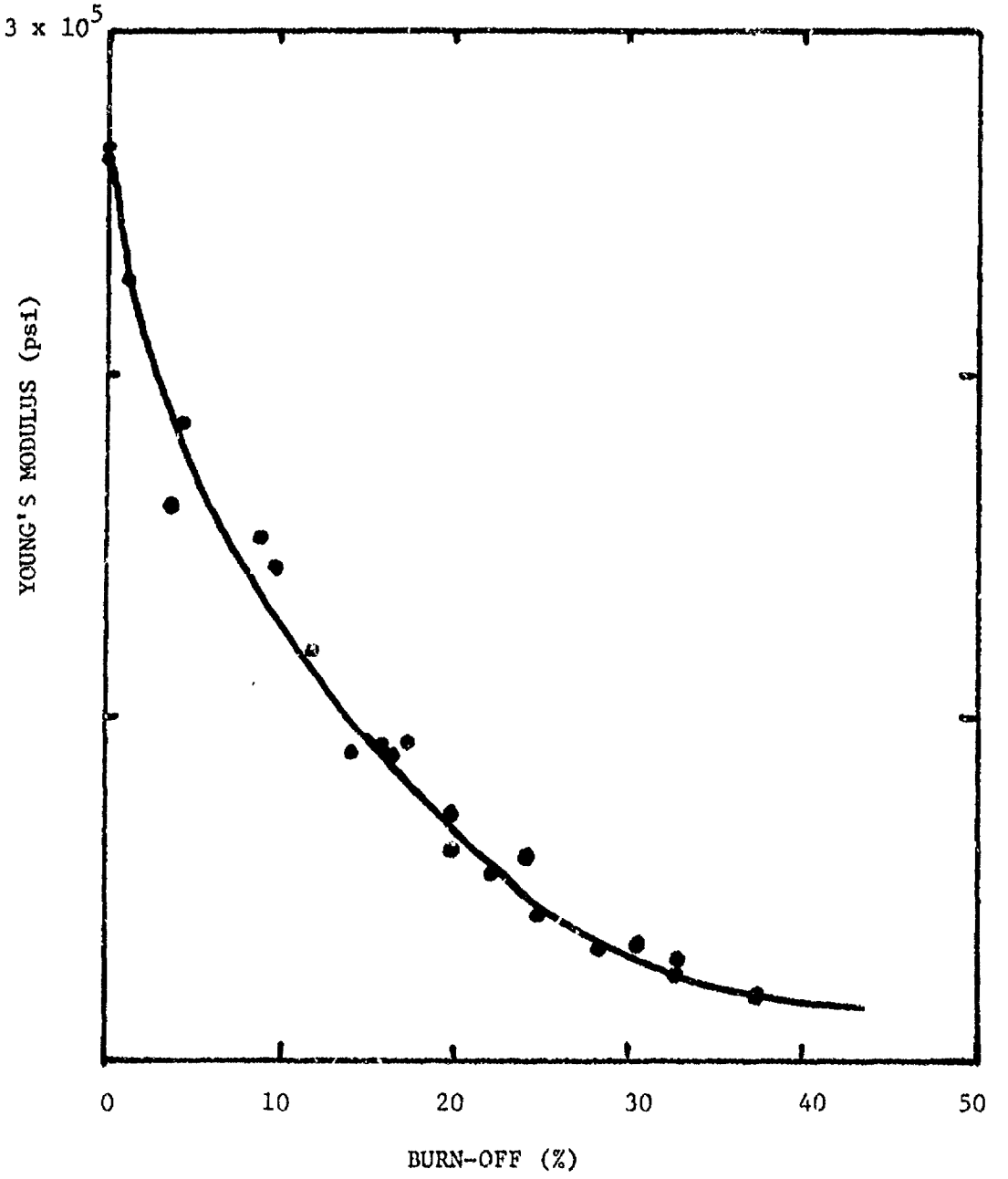

Figure 7: Young's Modulus as a function of burn-off for low-Ca material oxidized in air.

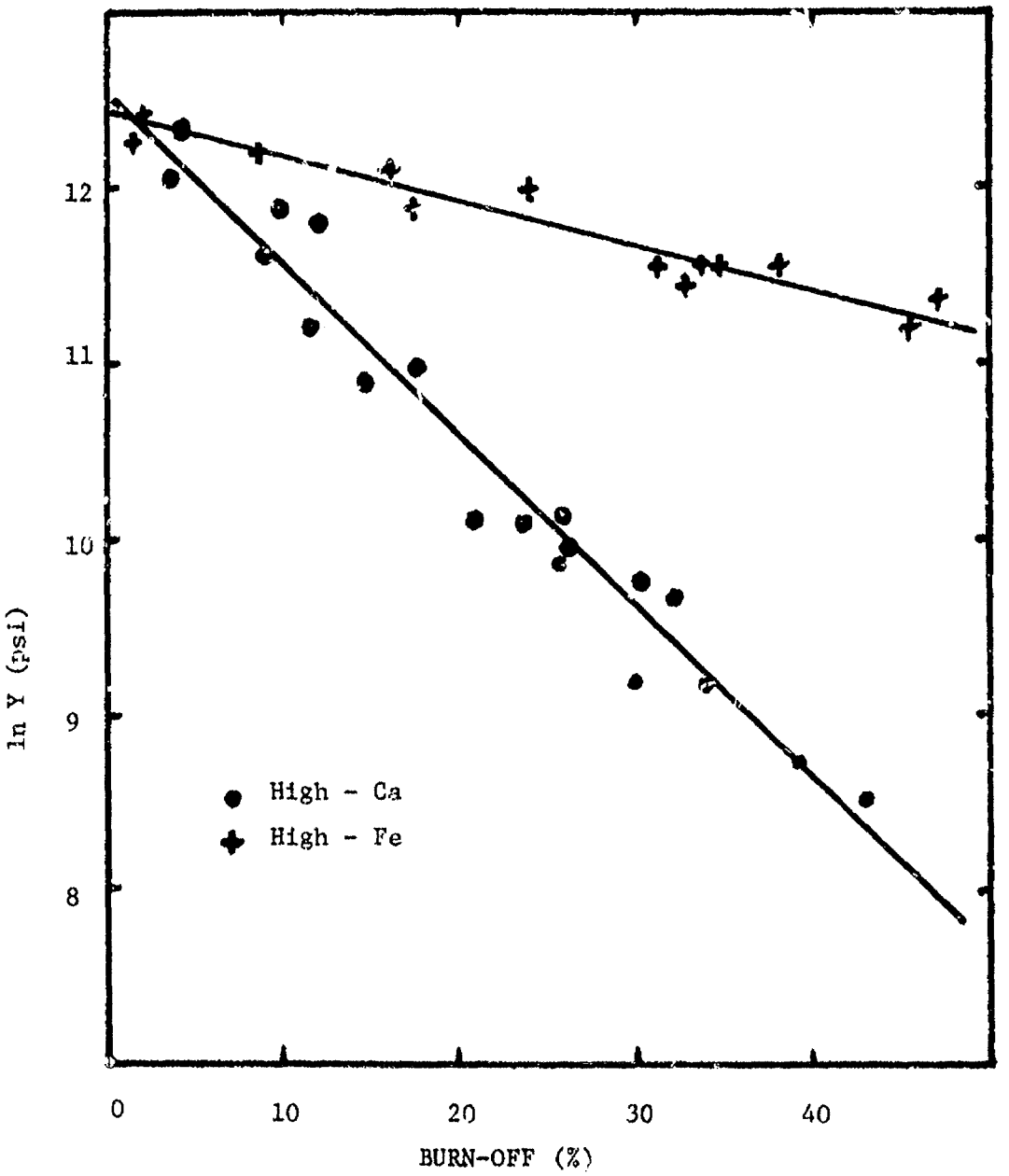

Figure 8: Logarithm of Young's Modulus as a function of burn-off for materials oxidized in H_2O.

TABLE VI

Values of η in the expression $Y/Y_o = \exp(-\eta\beta)$

Material	CO_2	Air	H_2O
Low Fe	0.030+	0.042	0.025
High Fe	0.030+	0.046	0.025
Low V	0.104	0.065	0.051
High V	0.069	0.040*	0.084
Low Ca	0.091	0.069	0.038
High Ca	0.055+	0.089	0.093

+ Values were higher for burn-offs greater than 25%.

* Data very scattered.

TABLE VII

Burn-off (%) Required to Produce a 50% Loss in Young's Modulus

Material	CO_2	Air	H_2O
Low Fe	20	12	20
High Fe	21	13	20
Low V	7	8	10
High V	9	10	9
Low Ca	5	7	6
High Ca	7	6	6

in the 12-15% range for each oxidant were therefore examined using the mercury porosimeter.

Some typical curves of total porosity and pore spectra are shown in Figures 9 and 10 for the high V material. In this case only ~15% of the porosity generated in air and H_2O has a diameter greater than 2 μm, while for CO_2 the corresponding value is over 40%. For the low V material, the values are approximately the same. There is no obvious relationship between these data and the changes in mechanical properties shown in Tables IV and V and the same can be said for all the other materials. Obviously the mechanical property changes are not simply due to total porosity increases, otherwise the changes would simply be a function of burn-off. Neither, from these results, are they simply a function of porosity size distribution. One must therefore conclude that spatial distribution is of major importance. For this reason it was thought that scanning electron microscope examination would provide possible useful information to help interpret the mechanical property data.

4. Scanning Electron Microscopy

Examination of the materials in the scanning electron microscope immediately showed that more gross internal porosity was produced in the Fe-samples in all oxidants than in any of the other materials. (Note that these materials had the highest initial density -- see Table I -- and thus the lowest porosity). This was clear at magnifications of less than 100x. Figures 11 and 12 (30x) are for high-Fe and high-V oxidized in CO_2 to burn offs of 40% and 55% respectively. Even with the higher burn-off in the high-V material there is less evident large porosity. In the Fe-materials the amount of gross porosity visible at this magnification (30x) varied according to oxidant used, with H_2O producing much more than either air or CO_2 which were about equal in their effect.

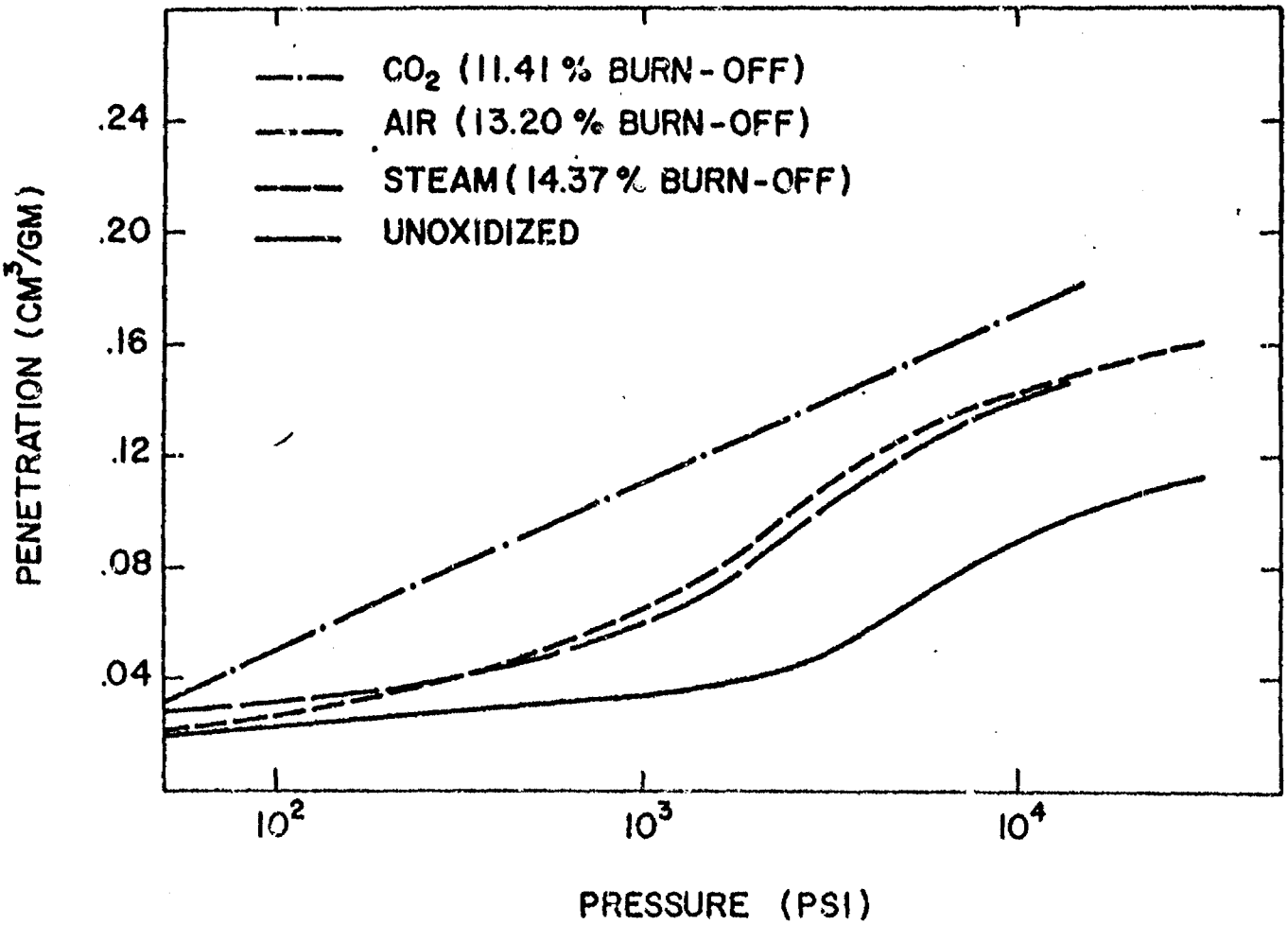

Figure 9. Porosity of 95-44 (high-V) as a function of mercury porosimeter pressure for different oxidation conditions.

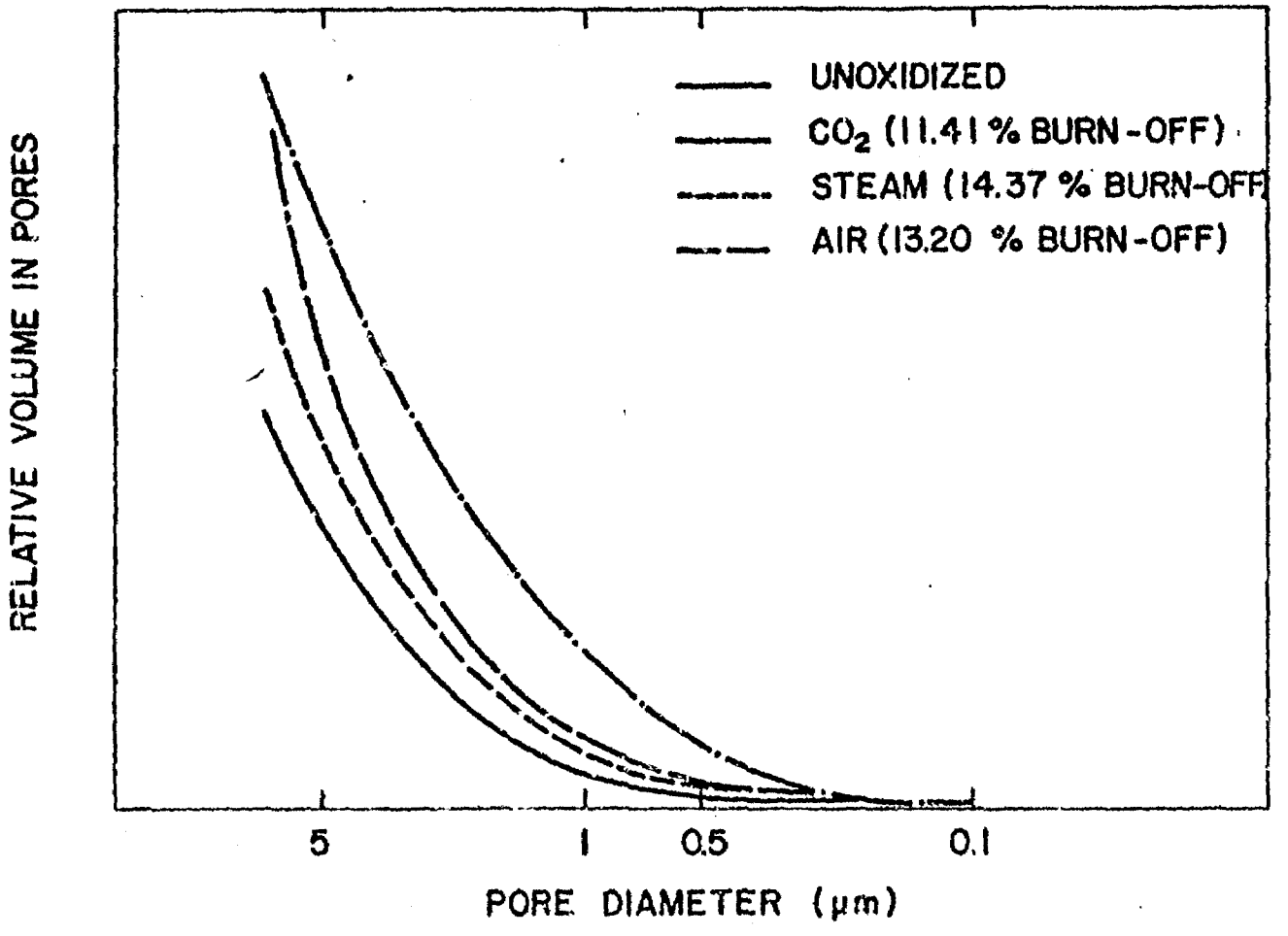

Figure 10. Pore size distribution of 95-44 (high-V) oxidized in CO_2, air and steam.

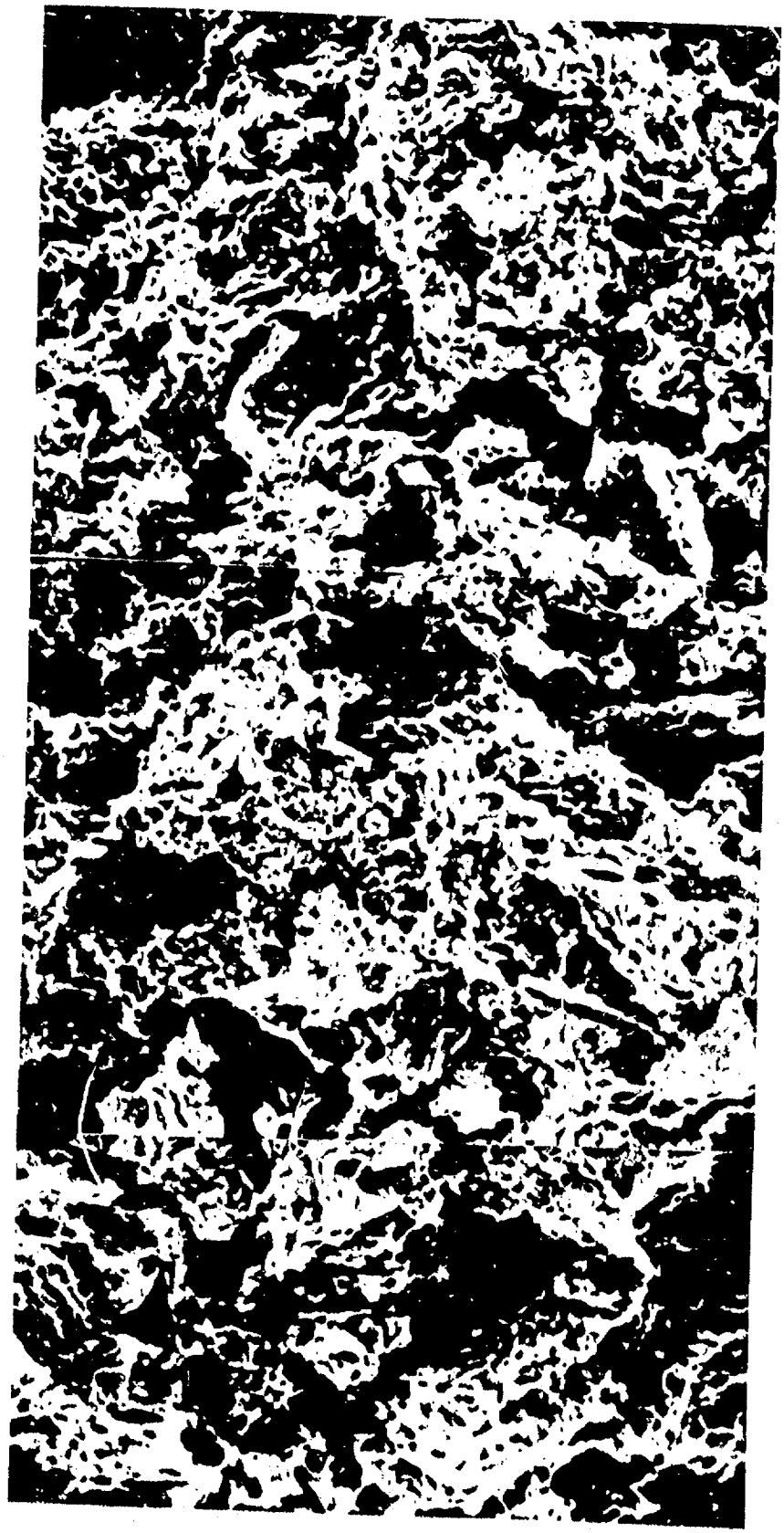

Figure 11. Scanning electron micrographs of 91-25 (high-Fe) oxidized in CO_2 to 44.00% burn-off.

Figure 12. Scanning electron micrographs of 95-44 (high-V) oxidized in CO_2 to 55.15% burn-off. (30X)

Comparing these observations with the mechanical property data it is evident that oxidation which produces gross pores has less effect on mechanical properties than does oxidation which produces a dispersion of smaller pores. Strength reductions for the Fe-bearing materials were much greater for oxidations in CO_2 and air than for H_2O, and in all cases were less than for Ca- and V-bearing materials. The physical reality of these results is that removing a filler particle, or grain, has little effect whereas the removal of the much finer intergranular binder produces significant weakening. While the observations appear to fit these facts it should be remembered that the iron was added via the binder and the calcium and vanadium via the filler so that if anything one might have expected the microscope observations to be reversed.

Higher magnification examination showed that in many cases, especially the Ca- and V- materials, fracture occurred via cleavage of the graphite crystals on planes which had suffered severe oxidation. The planes often contained circular oxidation pits several microns in diameter (Figure 13) and channels characteristic of catalytic attack were also sometimes visible (Figure 14). However in the Fe-materials severe roughening of the edges of the layer planes was observed (Figure 15), quite different from what was observed in other materials (Figure 16).

There was evidence that oxidation occurred preferentially in the binder in the Ca- and V- materials. In Figure 17 a filler particle in high-Ca material oxidized in CO_2 is clearly visible through a very "moth-eaten" binder. However some filler particles were seen in Ca-material oxidized in H_2O which had suffered extensive internal oxidation, resulting in a spongy interior (Figure 18). It is interesting to note that there are no obvious signs of impurity particles in these instances, while whenever a clump of impurity was seen, and identified as such using energy dispersive x-ray analysis, there was no obvious enhanced local oxidation.

Figure 13. Scanning electron micrographs of 95-37 (low-V) oxidized in CO_2 to 57.20% burn-off. (2000X)

Figure 14. Pitted filler particle surface of high calcium-containing graphite oxidized 38% in CO_2 (500 X).

Figure 15. Scanning electron micrographs of 91-25 (high-Fe) oxidized in H_2O to 53.20% burn-off showing gross pitting and rough edges. (800X)

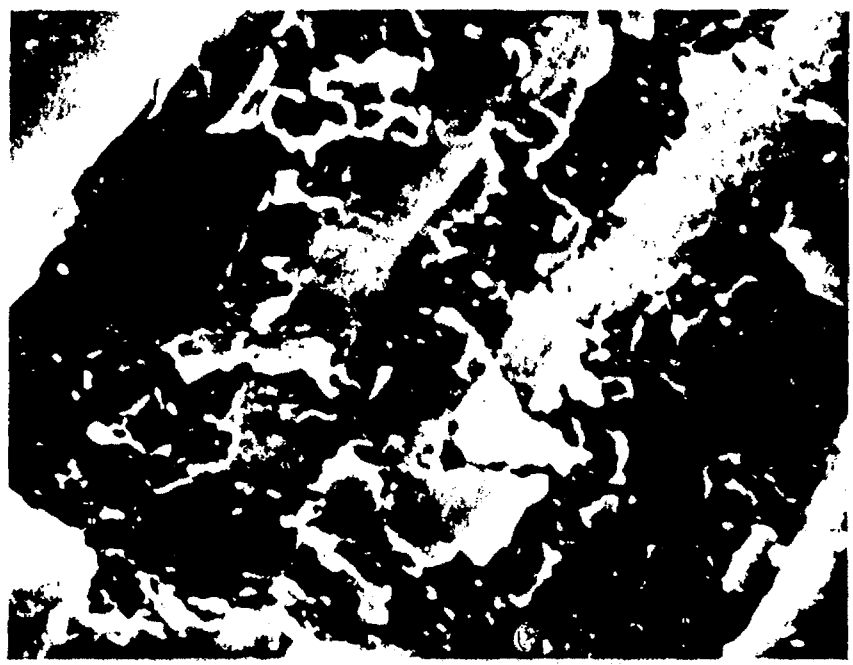

Figure 16. Scanning electron micrographs of 95-44 (high-V) oxidized in H_2O to 10.78% burn-off showing pitting and channeling at edges. (2000X)

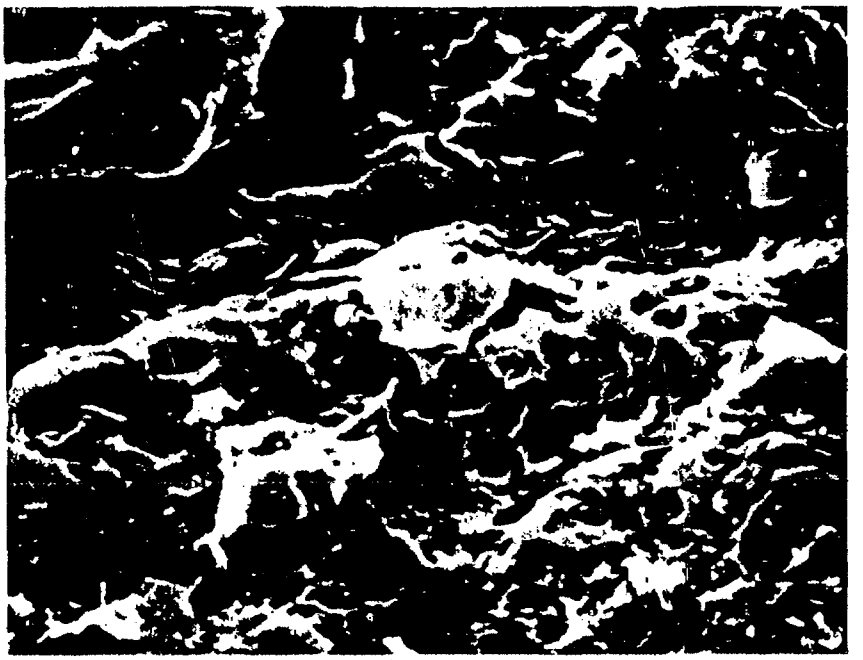

Figure 17. Fracture surface of high calcium containing oxidized 38% in CO_2. Filler particle (upper left) is visible underneath the remaining severly oxidized binder (1000 X).

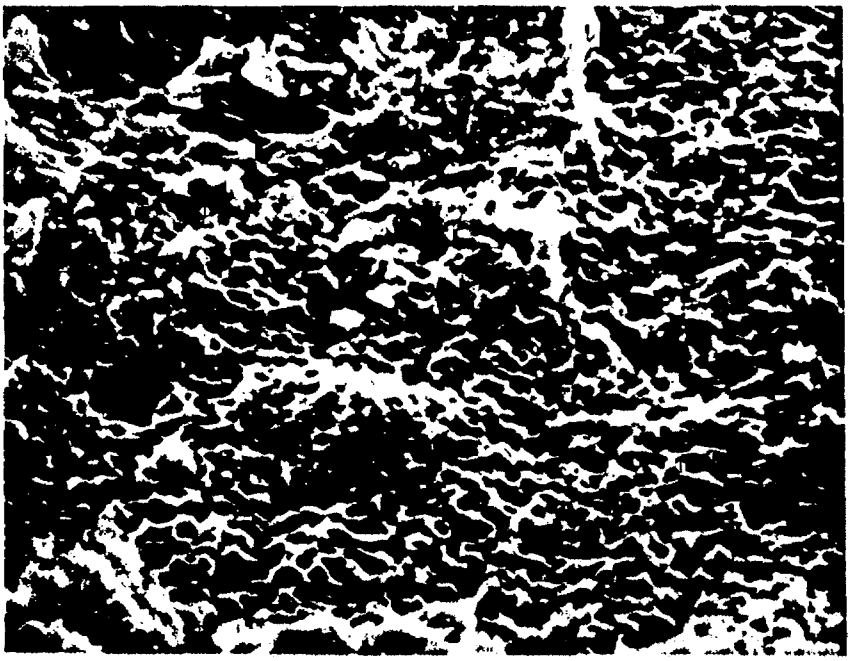

Figure 18. Fractured filler particle in high calcium-containing graphite oxidized 32% in H_2O (500 X).

5. Discussion

The results on mechanical property changes shown in Tables IV - VII show that there are very real effects of, and significant differences between, the various catalytic dopants. However within the concentration range examined there appears to be little effect of impurity concentration. For example 50 and 200 ppm of calcium are equally effective in the effects measured.

As far as catalytic effects are concerned, by far the most important seen here was the effect of Ca on H_2O oxidation. Not only did this cause much higher oxidation rates for a given temperature and H_2O concentration, but when these parameters were reduced in order to obtain a comparable oxidation rate, the effect on loss of strength and Young's modulus was most severe. Indeed in this respect Ca was equally effective in air and almost as effective in CO_2.

While Fe was added via the binder and V and Ca via the filler, oxidation appeared to occur in the other microconstituent. There is no reason to think other than that the impurities were uniformly distributed throughout the material as a consequence of the graphitization. Indeed diffusion of a large proportion of the impurity through the graphite must have occurred to account for the large loss of additive during processing. The reason for the observation is therefore not clear unless Fe tends to segregate to certain regions in the material. In any event it is clear that the smaller strength and modulus reductions in the Fe materials as a result of oxidation are associated with the production of gross porosity rather than a fine intergranular porosity such as seen in the other materials.

The severe effect of H_2O on the calcium-doped materials may be associated with severe internal weakening of some of the filler particles, while the preferential oxidation of binder is also a major factor.

In spite of the attempt to isolate one specific impurity for each sample,

it is evident from Table II that other impurities were present. There is no evidence that these were important or that there were any synergistic effects.

Finally, it is interesting to note that while it was much easier to achieve uniform oxidation in CO_2 than in H_2O and air, it was in this reactant that plots of the logarithm of Young's modulus versus burn-off split into two linear regions. There are no explanations for this.

C. Final Comments and Summary

During the course of this study it was hoped to examine in the transmission electron microscope some highly oriented pyrolytic graphites which had been irradiated at very high temperatures. These irradiations have still not been performed, but the specimens will be examined when, and if, they are ever received.

Earlier work during the term of this contract has shown: that there is no enhancement of graphite oxidation rates when compressive stress is applied; that the effect of gas flow rate past the sample on the oxidation rate is more complicated than usually thought; and that the microstructure of graphite is of great importance in determining the effects of oxidation on compressive strength. Work performed in the final stage of this contract has highlighted the effects of different impurities on both oxidation rates and degredation in compressive strength and modulus. In this last respect it is evident that for the conditions likely to be encountered in high temperature nuclear reactors, helium coolant contaminated with H_2O vapor, calcium is a much more important impurity than either iron or vanadium. This fact is contrary to what is often believed, i.e. that iron is the most important impurity in reactor graphites as far as oxidation is concerned.